Rotated Global Modes of Non-ENSO Sea Surface Temperature Variability

ALBERTO M. MESTAS-NUÑEZ

Cooperative Institute for Marine and Atmospheric Studies, University of Miami, Miami, Florida

DAVID B. ENFIELD

NOAA/Atlantic Oceanographic and Meteorological Laboratory, Miami, Florida

(Manuscript received 16 July 1998, in final form 30 December 1998)

ABSTRACT

A varimax rotation was applied to the EOF modes of global SST derived by Enfield and Mestas-Nuñez. The SST anomaly record is more than a century long, with a global complex EOF representation of ENSO and a linear trend removed at every grid point. The rotated EOF modes capture localized centers of variability that contribute to the larger-scale spatial patterns of the unrotated modes. The first rotated EOF represents a multidecadal signal with larger response in the North Atlantic. The second rotated EOF represents an interdecadal fluctuation with larger response in the eastern North Pacific and out of phase fluctuations of smaller amplitude in the central North Pacific. The third rotated EOF captures interdecadal fluctuations in the eastern tropical Pacific with a dominant peak that coincides with the 1982/83 ENSO. The fourth rotated EOF has interdecadal to multidecadal nature with larger response in the central equatorial Pacific and quasi-symmetric out-of-phase response in the western North and South Pacific. The fifth mode represents multidecadal fluctuations with large response at about 40°N in the North Pacific. The sixth mode has interannual to interdecadal timescales with largest response confined to the South Atlantic. The authors' rotated modes are dominated by intra- rather than interocean fluctuations supporting the hypothesis that the non-ENSO variability is more regional than global in nature. Analyses of sea level pressure and surface wind stress show that in general the non-ENSO rotated EOFs are consistent with an ocean response to local atmospheric forcing. An exception is the eastern tropical Pacific mode, which is more consistent with an atmospheric response to changes in the ocean SST.

1. Introduction

We have recently analyzed more than a century of global SST anomalies (SSTA) by separating their nonseasonal variability into ENSO and non-ENSO components (Enfield and Mestas-Nuñez 1999). The dominant ENSO signal was extracted using a complex version of EOF analysis that allows for phase propagation. The residual non-ENSO variability was detrended and investigated using ordinary (conventional) EOF analysis. The three leading modes of the non-ENSO residuals were related to slow climatic signals described in the literature. The first two modes both had decadal-to-interdecadal timescales with high response in the Pacific and smaller but significant response in other basins. The third mode was a multidecadal signal with maximal realization in the extratropical North Atlantic, anticorrelated across the intertropical convergence zone, and having strong variability of opposite phase in the eastern tropical Pacific.

Corresponding author address: D. B. Enfield, NOAA/AOML, 4301 Rickenbacker Causeway, Miami, FL 33149.
E-mail: enfield@aoml.noaa.gov

The goal of this paper is to investigate the presence of localized or regionalized centers of SSTA variability in the non-ENSO residuals, which can be used to define useful climatological indexes. Because EOFs are designed to efficiently describe the global variance of the data, they generally do not represent a large fraction of the variance in any given region. Regionalization, however, can be accomplished by linearly transforming the EOFs through a varimax orthogonal rotation. Here we apply a varimax rotation to the ordinary EOFs of Enfield and Mestas-Nuñez (1999) and describe the dominant rotated modes (REOFs). We compare the EOFs with the REOFs and investigate the relation of the REOFs with sea level pressure and surface wind stress.

Kawamura (1994) presented global REOFs of SSTA using data from the U.K. Meteorological Office for a 34-yr period extending from January 1955 to December 1988. He divided each SSTA time series by its standard deviation and no time filtering was applied before rotation. The main differences between our study and Kawamura's are: we use a longer SSTA record (136 yr), we remove ENSO and the secular trend because they are global in nature and therefore we believe that they should be removed before regionalization, we do not

divide the time series by their standard deviations, we remove high-frequency (intraseasonal) variability and we use a different normalization of the EOFs before rotation.

Our analysis is more similar to earlier analyses developed to predict Sahel rainfall variations by Folland et al. (1991) and Ward et al. (1993) (hereafter F91W93). F91W93 performed an EOF analysis of seasonally averaged $10° \times 10°$ SSTA from the U.K. Meteorological Office for the period 1901–80. Their EOFs 1–3 captured the global warming signal, the ENSO signal, and a pattern similar to the Atlantic multidecadal EOF 3 of Enfield and Mestas-Nuñez (1999), respectively. Arguing that these EOFs had a global nature F91W93 did not include them in a varimax rotation of modes 4–13. Therefore, they effectively removed representations of global warming and ENSO but using a different method than ours. In this study, we do not remove other global signals before rotation because it is not well known if other empirical modes such us the third mode of F91W93 and Enfield and Mestas-Nuñez (1999) represent actual global climatic signals.

A description of the data preparation is given in section 2. The results of the varimax rotation are presented in section 3 where the space–time structure of the leading rotated modes are described and compared to the unrotated modes. The connection of these modes with surface atmospheric fields is presented in section 4 and a final summary and discussion is given in section 5.

2. Data

a. Sea surface temperature

The non-ENSO SSTA used in this study come from the global analyses generated by Kaplan et al. (1998) (hereafter K)—for a brief description see Enfield and Mestas-Nuñez (1999). The input to the K analyses are ship observations from the MOHSST5 version (Parker et al. 1994) of the Global Ocean Surface Temperature (GOSTA) data set (Bottomley et al. 1990). This is a newer version of the U.K. Meteorological Office dataset than the ones used by Kawamura and F91W93. This version incorporates the Comprehensive Ocean–Atmosphere Data Set (COADS) compilation (Woodruff et al. 1987). The SSTA are monthly deviations from the GOSTA 1951–80 climatology, for the period 1856–91 (i.e., 1632 time points). They are gridded in $5° \times 5°$ boxes with a total of 1207 grid points.

A detailed account of the processing applied to the K data to separate ENSO and non-ENSO components are given in Enfield and Mestas-Nuñez (1999). Briefly, ENSO was defined as the leading complex (Hilbert transform) EOF of the bandpassed data on the 1.5–8-yr band. This representation of ENSO was calculated and removed from a version of the K data that were previously low passed to filter out periods shorter than 1.5 yr. Finally, a linear trend was removed at every grid point. The ENSO representation explains 17% and the trend 9% of the total variance after the 1.5-yr filtering. The residual SSTA data contain interannual to multidecadal timescales and their spatio–temporal variabilities have no commonality with the 136 yr of interannual ENSO variability.

TABLE 1. Percentage of low-passed and detrended SSTA variance explained by the first 10 unrotated and rotated non-ENSO EOFs.

Mode	Unrotated	Rotated
1	12.6	7.3
2	11.1	7.1
3	7.2	6.9
4	5.3	6.9
5	5.0	6.1
6	4.2	5.5
7	3.9	5.2
8	3.3	5.2
9	3.0	4.3
10	2.9	4.2
Total	58.6	58.6

Enfield and Mestas-Nuñez (1999) studied the non-ENSO SSTA variability using ordinary EOFs. In this study we perform a varimax rotation of these EOFs using the first 10 modes. The number of EOFs to retain for rotation is somewhat arbitrary, here we use 10 EOFs for consistency with Kawamura (1994). Our first 10 modes explain 59% of the global low-passed and detrended variance in the non-ENSO data. Relative to the global unfiltered variance, our 10 modes explain a smaller fraction (23%) than Kawamura's (36%). As noted in the introduction, Kawamura worked with unfiltered data. In contrast, we removed intraseasonal fluctuations, ENSO, and local trends (in that order) from the K data. Relative to the unfiltered K data, intraseasonal fluctuations explain 43% of the total variance, ENSO 10%, trend 5%, and low-passed and detrended non-ENSO variability the remainder 42%.

The modal distributions of global low-passed and detrended SSTA variance explained before and after rotation are shown in Table 1. For comparison with Enfield and Mestas-Nuñez (1999), the distributions of low-passed SSTA variance explained before removing the trend can be calculated by multiplying the figures in Table 1 by 0.7. For comparison with Kawamura (1994, his Table 1), the modal distributions of unfiltered variance can be obtained by multiplying the figures in Table 1 by 0.4.

Our four leading REOFs account for less unfiltered global variance (2.8%–2.9%) than Kawamura's (3.5%–8.3%) because Kawamura's REOFs include ENSO and global warming, which are global phenomena. The variance explained by our ENSO mode can be compared with other authors's representations of ENSO such as Kawamura's first REOF, F91W93's second unrotated EOF, and Hsiung and Newell's (1983) first unrotated EOF. The fraction of global unfiltered variance explained by our ENSO mode is about 10%, which is

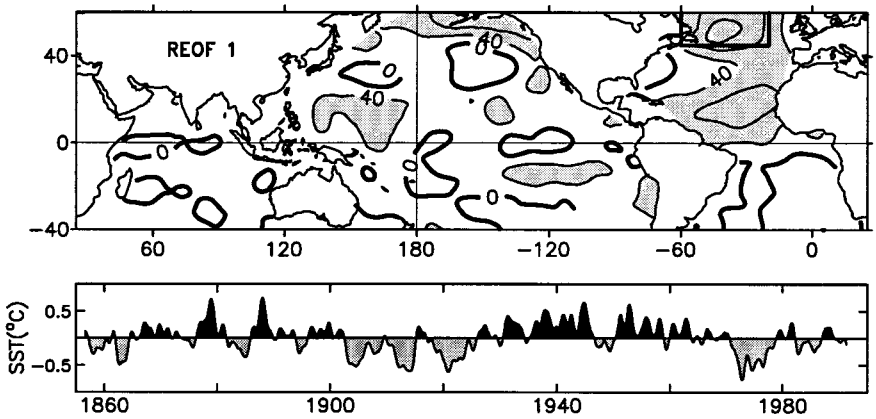

FIG. 1. First rotated EOF (REOF) of the non-ENSO dataset, describing the North Atlantic multidecadal mode. Upper panel: spatial distribution of the response with respect to the modal reconstruction over the index region (rectangle); contour interval is 40 and a score of 100 is the response of the data average over the index region. Regions with scores greater than 40 are lightly shaded and smaller than −40 are heavily shaded. Dashed contours are negative. Lower panel: temporal reconstruction of the mode related variability averaged over the index region.

consistent with the 8.3% of Kawamura's, 7.8% of F91W93's, and 7.7% of Hsiung and Newell's. The fact that our ENSO explains more variance may be partly due to our complex EOF (CEOF) representation capturing more ENSO signal in a single mode.

The second REOF of Kawamura captures a trend with space pattern similar to the distribution of the linear (least squares) trend in the K dataset (see Fig. 1 of Enfield and Mestas-Nuñez 1999). Therefore, we believe that Kawamura's REOF 2 is related to the global warming signal he did not remove. Note that Kawamura's REOF 2 accounts for 4.9% of the unfiltered variance, which is consistent with the 5% accounted by our estimate of the trend.

The orthogonality properties of the REOFs depend on the way that the EOFs are normalized. However, it is not possible to preserve orthogonality in time and space simultaneously (Jolliffe 1995). In this study, we use the following normalization: the space patterns are unit length eigenvectors and the time series are eigenvectors multiplied by square root of eigenvalues. This choice allows us to preserve orthogonality in space but relaxes orthogonality in time so that the REOFs are not constrained to be temporally uncorrelated, as was the case in the study of Kawamura (1994). Therefore the normalization used in this study has the effect of not prejudicing conclusions regarding the possibility of couplings between rotated modes, especially those representing subregions of the same ocean basin.

b. Sea level pressure and wind stress

The meteorological fields of sea level pressure (SLP) and surface vector wind stress used in this study come from the version of the COADS dataset produced at the University of Wisconsin—Milwaukee (UWM) by da Silva et al. (1994). This dataset (referred to as the UWM/COADS dataset) consists of monthly $1^\circ \times 1^\circ$ objectively analyzed fields for the period 1945–93. We calculated long-term average seasonal cycles (using the same period of the GOSTA climatology) and removed them to generate seasonal anomalies of SLP and wind stress.

The SLP and vector wind stress anomalies were composited with respect to the antipodal phases of each time series of the non-ENSO REOFs. The UWM/COADS data include corrections to reduce wind speed bias and artificial trends known to exist in the COADS data (e.g., Cardone et al. 1990). However, we also performed the analyses using SLP and (uncorrected) surface vector winds from COADS for the period beginning in 1950 (not shown) and obtained very similar results to the ones presented in section 4.

3. Rotated modes of SSTA variability

In the following sections we present and describe the six leading non-ENSO REOF modes (R1–R6) and compare them with the three EOF modes (U1–U3) of Enfield and Mestas-Nuñez (1999). Each REOF mode is presented as a two-panel figure (Figs. 1–6) with the spatial pattern at the top and the temporal realization at the bottom. The temporal realization is the spatial average over a reference region of the modal reconstruction of the SSTA (units of temperature). This is equivalent to multiplying the REOF amplitude time series with the average of its spatial eigenfunction in the reference region. This scaling does not change the character of the time series. Indeed, the correlation between each of the time series in Figs. 1–6 and its corresponding REOF amplitude time series is one. The reference regions are chosen to enclose an area of large spatial amplitude and are indicated with rectangular boxes in the upper panel

TABLE 2. Temporal correlations of the temporal realizations of the unrotated (*U*) and rotated (*R*) modes with the data indexes.

*U*1	*U*2	*U*3	*R*1	*R*2	*R*3	*R*4	*R*5	*R*6
0.71	0.69	0.75	0.84	0.85	0.88	0.82	0.92	0.92

of each figure. The spatial pattern is constructed from the regression coefficient between the temporal realizations and the low-passed and detrended non-ENSO SSTA data.

The first three unrotated modes explain 31% of the total low-passed and detrended variance as opposed to 40% of the first six rotated modes (Table 1). However, no pair of rotated modes approaches the variance explained by the first two unrotated modes because the rotated modes are regional representations whereas the unrotated modes have an interocean character to them. The temporal correlation of the first three EOFs (not shown) and the first six REOFs with data indexes calculated by averaging the SSTA over the reference regions are given in Table 2. By squaring these correlations one can see that the rotated modes explain more local variance (67%–85%) than the unrotated modes (48%–56%). The temporal and spatial correlations between the unrotated and rotated modes are given in Tables 3 and 4.

Enfield and Mestas-Nuñez (1999) have described in detail the first three unrotated modes of variability (see their Figs. 3, 4, and 5) and their associations with Northern Hemisphere teleconnection patterns. Briefly, U1 and U2 have decadal-to-multidecadal timescales with high responses in the Pacific. The U3 is a multidecadal signal with maximal realization in the extratropical North Atlantic southeast of Greenland. Modes U1, U2, and U3 appear to be related to the following 500-hPa pressure height midtropospheric patterns: Pacific North American (PNA), North Pacific (NP), and the Arctic Oscillation/North Atlantic Oscillation (AO/NAO), respectively.

The final set of statistics presented in this study are the correlations between the time series of the rotated modes (Table 5). As discussed in section 2a, the rotated modes are not constrained to be temporally uncorrelated with each other. Indeed the temporal correlations between the rotated modes shown in Table 5 are in the 0.01–0.4 range.

TABLE 3. Correlations of the temporal realizations of the unrotated (*U*) and rotated (*R*) modes.

	*R*1	*R*2	*R*3	*R*4	*R*5	*R*6
U1	0.60	0.75	0.66	0.34	−0.33	0.16
U2	0.22	0.01	0.03	−0.75	0.62	0.55
U3	0.59	0.15	−0.51	−0.04	0.10	−0.36

TABLE 4. Correlations of the space patterns of the unrotated (*U*) and rotated (*R*) modes.

	*R*1	*R*2	*R*3	*R*4	*R*5	*R*6
*U*1	0.56	0.83	0.69	0.62	−0.67	−0.24
*U*2	−0.06	−0.35	−0.33	−0.91	0.78	0.58
*U*3	0.73	0.21	−0.50	−0.04	0.11	−0.38

a. Mode 1: North Atlantic multidecadal variability

The first REOF (R1, Fig. 1) has a multidecadal nature with superimposed interannual fluctuations and large spatial response in the high latitudes of the North Atlantic just south of Greenland. Amplitudes nearly as strong are found in the tropical North Atlantic between 10° and 20°N and in the Gulf of Alaska. Secondary regions of moderate response are found in the eastern tropical South Pacific and in the western tropical North Pacific.

As seen in the first column of Tables 3 and 4, R1 is temporally and spatially correlated with U1 and U3. Mode R1 accounts for the tropical North Atlantic response of both of these unrotated modes. For U1, the absence of high positive response in the northern North Atlantic indicates that other rotated modes should also be important contributors to U1 variability. Inspection of the first row of Tables 3 and 4 confirms that this is the case and shows large contributions by R2 and moderate contributions by modes R3–R5. For U3, the importance of rotated modes other than the first is evidenced by the presence of regions of moderate to high negative U3 response in the eastern tropical Pacific and in the South Atlantic. The third row of Tables 3 and 4 shows that these structures may come from rotated modes 3 and 6.

As described above, R1 (Fig. 1) has large positive response in the North Atlantic and insignificant response in the South Atlantic. This structure is very similar to rotated mode 3 of Kawamura (1994) obtained from data for a shorter period (1950s–1980s). Regions of anticorrelated SSTA variability across the Atlantic ITCZ, as in the case of U3, define what is known as the Atlantic dipole. If dipole variability were a dominant component of the Atlantic SSTA variability, it should be captured by a single REOF mode. However, this is not the case. Because R1 describes very well the northern but not at all the southern components of the U3 Atlantic dipole structure, the existence of an Atlantic dipole mode is

TABLE 5. Correlations between the time series of the rotated modes.

	*R*1	*R*2	*R*3	*R*4	*R*5	*R*6
*R*1	1.00	0.30	0.17	0.01	−0.03	0.02
*R*2		1.00	0.26	0.19	−0.18	0.08
*R*3			1.00	0.19	−0.11	0.16
*R*4				1.00	−0.38	−0.26
*R*5					1.00	0.10
*R*6						1.00

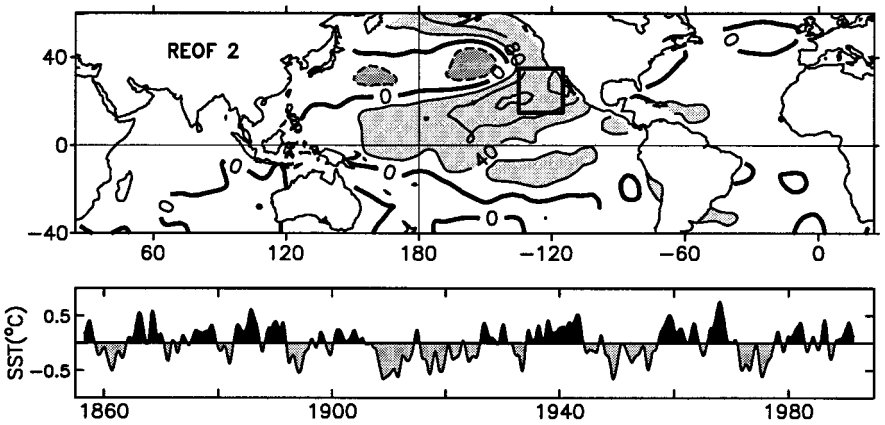

FIG. 2. As in Fig. 1: Second REOF of the non-ENSO dataset, describing the eastern North Pacific decadal variability.

called into question. This issue is discussed further in section 3f where we decribe the R6 mode.

Mode R1 clearly captures the essence of the North Atlantic SST variability that Enfield and Mestas-Nuñez (1999) related to the AO/NAO-like tropospheric variability. The region of positive response in the Gulf of Alaska that was present in U3 remains and is stronger in R1. As noted by Enfield and Mestas-Nuñez (1999), this is suggestive of a tropospheric ''bridge'' between the North Atlantic and the Gulf of Alaska. This notion is reinforced by the fact that the two areas do not separate under rotation.

b. Mode 2: Eastern North Pacific interdecadal variability

The second REOF (R2, Fig. 2) has interdecadal nature with large positive amplitudes in the eastern North Pacific at about 25°N. This region of large response extends northward along the coast of the United States and then westward into the subpolar North Pacific. A region of moderate amplitude and opposite phase is found in the central North Pacific and regions of moderate amplitude and same phase are found in the eastern tropical South Pacific and in the western tropical North Atlantic, including the Caribbean Sea.

Mode R2 is temporally and spatially correlated with U1, as seen in the second column of Tables 3 and 4. However, it does not account for the moderate amplitudes of U1 in the North Atlantic, which we attribute to R1. Enfield and Mestas-Nuñez (1999) suggested that U1 may share the same mechanism as the (removed) secular warming because they have similar spatial patterns. Since R2 is the mode that best describes the spatial structure of U1 (see first row of Table 4), the same connection with the secular warming can be proposed for R2. Furthermore, because R2 is more confined to the eastern North Pacific than U2, one can say that a possible connection with the secular warming may be restricted to the eastern North Pacific Ocean.

Mode R2 captures the core essence of the Pacific interdecadal variability described in many papers (e.g., Trenberth and Hurrel 1994; Miller et al. 1994; Deser et al. 1996; Latif and Barnett 1996; Mantua et al. 1997; Nakamura et al. 1997; Zhang et al. 1997; Giese and Carton 1999) and referred to as the Pacific Decadal Oscillation (PDO). One hypothesis that has been proposed to explain the structure of the PDO involves the subduction of subtropical waters and their advection and upwelling at lower latitudes on decadal timescales (Deser et al. 1996; Gu and Philander 1997). The spatial structure of R2 indicates that the origin of the PDO may be in the midlatitude eastern North Pacific.

The PDO-like characteristics of R2 cannot be mentioned without reference to ENSO. The Pacific spatial pattern evident in U1, R2, and in other papers on the PDO is very similar to the ENSO pattern, but less confined to the low latitudes and extending farther to the west than ENSO. Moreover, Enfield and Mestas-Nuñez (1999) found that the 500-hPa correlation pattern for U1 looks very similar to the midtropospheric (PNA) teleconnection pattern that others have related to ENSO. Whether or not ENSO and the PDO are connected in some way, or simply resonate in a similar manner, remains the subject of ongoing research.

c. Mode 3: Eastern tropical Pacific interdecadal variability

The third REOF of non-ENSO variability (R3, Fig. 3) has a large amplitudes in the eastern tropical Pacific with a region of high positive response on the equator, extending southward along the coast of South America. A large region of moderate positive response is found in the Indian Ocean near the west coast of Australia. Small regions of moderate negative response are found in the North Atlantic just south of Greenland and in the western North and central South Pacific. This mode is spatially and temporally correlated with U1 and anticorrelated with U3 (column 3 of Tables 3 and 4). The

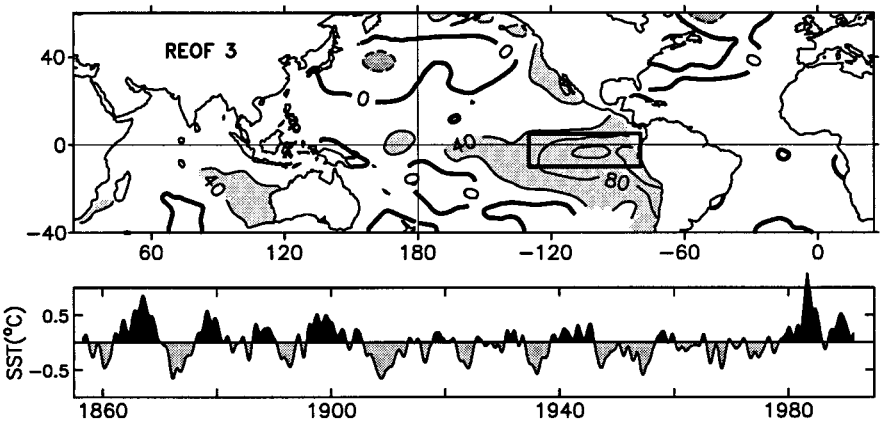

FIG. 3. As in Fig. 1: Third REOF of the non-ENSO dataset, describing the eastern tropical Pacific decadal variability.

high response in the eastern tropical Pacific occupies the same region of negative response of U3 that was antipodal with the North Atlantic.

The dominant feature in the time series of R3 is the shift to positive values in the late 1970s with a sharp peak during 1983. This corresponds to warming in the eastern Pacific during that time and suggests that decadal variability had a significant contribution to the amplitude of the strong 1982/83 ENSO. The ENSO-like decadal shift to warmer eastern tropical Pacific in the late 1970s has been noted by other authors (e.g., Nitta and Yamada 1989; Zhang et al. 1997). In their analysis, Zhang et al. removed scales shorter than 6 yr. Here we show that the warming of the eastern tropical Pacific that begun in the late 1970s also involved shorter (interannual) timescales.

In essence, R3 captures an interdecadal modulation of ENSO as well as unusual aspects of ENSO not described by our canonical (complex EOF) representation. These explain why the (removed) ENSO representation does not show a dominant 1982–83 peak present in common SSTA ENSO indexes (e.g., Niño 3).

d. Mode 4: Central tropical Pacific interdecadal variability

The fourth REOF (R4, Fig. 4) has interdecadal to multidecadal periodicities with very large positive response in the central tropical Pacific, large negative response in the western extratropical North and South Pacific, moderate positive response in the southern Indian Ocean, and small or insignificant response in other regions. As seen in column 4 of Tables 3 and 4, this mode compares well with U2. However, R4 is not the only contributor to U2, as can be seen by the more multidecadal nature of U2 and its larger response in the northern North Pacific and in the midlatitude Atlantic.

The dipole structure of R4 between the central North Pacific and the central equatorial Pacific compares well with U2 and the second mode of Nakamura et al. (1997). Nakamura et al. related their mode with variability associated with the subtropical front. However, our modes (U2 and R4) also have significant response northward in the region of the subarctic front. Differences between our results and other studies of Pacific interdecadal var-

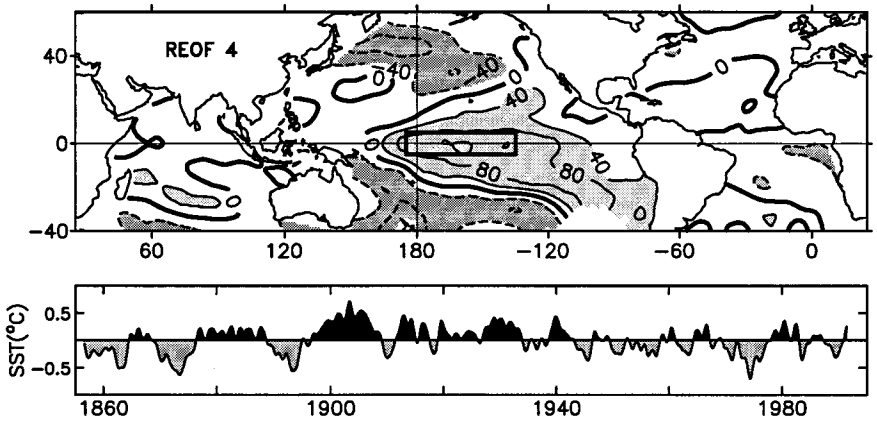

FIG. 4. As in Fig. 1: Fourth REOF of the non-ENSO dataset, describing the central tropical Pacific decadal variability.

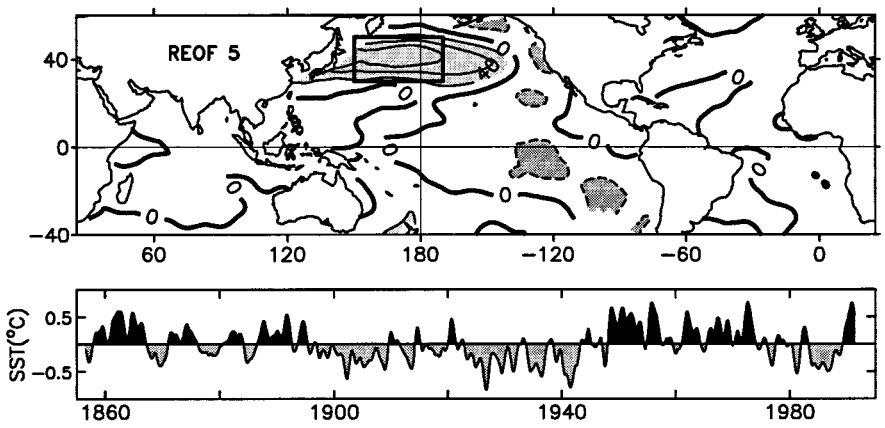

FIG. 5. As in Fig. 1: Fifth REOF of the non-ENSO dataset, describing the North Pacific multidecadal variability.

iability may be in part due to the different methods of analysis. Therefore some aspects of our interdecadal–multidecadal Pacific mode may be present in some of the papers cited when describing the PDO in section 3b. However, as noted by Enfield and Mestas-Nuñez (1999), there are enough differences between the Pacific interdecadal–multidecadal mode to suggest it should be treated separately from the interdecadal mode.

Mode R4 shows some indication of a shift to a warmer central equatorial Pacific during the 1970s but this is not as pronounced as in the eastern tropical Pacific, as described by R3. The lagged temporal crosscorrelation between R3 and R4 shows a maximum positive correlation (0.29) near zero lag but, surprisingly, a larger negative correlation (−0.47) with R4 leading R3 by 8.5 yr. Thus a prominent cooling in the central tropical Pacific would occur about nine years earlier than a warming in the eastern tropical Pacific, as is the case of the 1983 event.

Mode R4 has many aspects of the north Pacific multidecadal mode that Enfield and Mestas-Nuñez related to the NP tropospheric variability. The larger response in the central tropical Pacific and the more interdecadal nature of R4 indicate a tendency for the low latitudes to contribute the shorter timescales of the interdecadal–multidecadal mode.

e. Mode 5: North Pacific multidecadal variability

The fifth REOF of non-ENSO variability (R5, Fig. 5) has a multidecadal nature with very large positive response in the North Pacific and small amplitudes in the tropical and eastern extratropical Pacific. As in the case of R4, this mode compares well with U2 (column 5, Tables 3 and 4). Both R4 and R5 are major contributors to U2 (row 2, Tables 3 and 4). Mode R5 accounts for the larger response of U2 in the northern North Pacific but, similar to R4, has no contribution in the Atlantic.

Modes of North Pacific multidecadal variability similar to R5 were found by several authors using SSTA data for the period between the 1950s and the 1980s. For example, R5 compares well with the first mode of Nakamura et al. (1997) and Miller et al. (1994) from EOF analyses of the extratropical North Pacific. It also compares favorably with the second EOF of Deser and Blackmon (1995), who studied the Pacific north of 20°S, and with the second global rotated EOF of Kawamura (1994). Because both of these studies included the tropical Pacific, their first EOFs were dominated by ENSO variability. Consistent with Nakamura et al., the time series of R4 and R5 show that the mid-1970s cooling in the northern North Pacific occurred about two years earlier than the warming of the central tropical Pacific.

Mode R5 also compares well with the leading EOF of Mantua et al. (1997), who performed an EOF analysis of North Pacific SSTA since 1900. Their mode included anticorrelated variability in the central tropical Pacific. As seen in Fig. 5, R5 has very small response in the tropical Pacific. However, there is a significant correlation of −0.4 at zero lag (see Table 5) between the time series of R4 (central tropical Pacific decadal) and R5 (North Pacific multidecadal), which suggests some coupling between the two. Thus, R5 together with R4 appear to describe most of the aspects of the Pacific multidecadal mode (U2) of Enfield and Mestas-Nuñez (1999) that was related to the NP tropospheric variability.

f. Mode 6: South Atlantic interannual variability

The sixth REOF (R6, Fig. 6) has interannual to interdecadal timescales with large positive response in the northeastern and central South Atlantic, small positive response in the central North and South Pacific, and small negative response in the high-latitude North and South Atlantic.

This mode is positively correlated with U2 and to a lesser degree negatively correlated with U3 (see column 6 of Tables 3 and 4). It contributes to the moderate

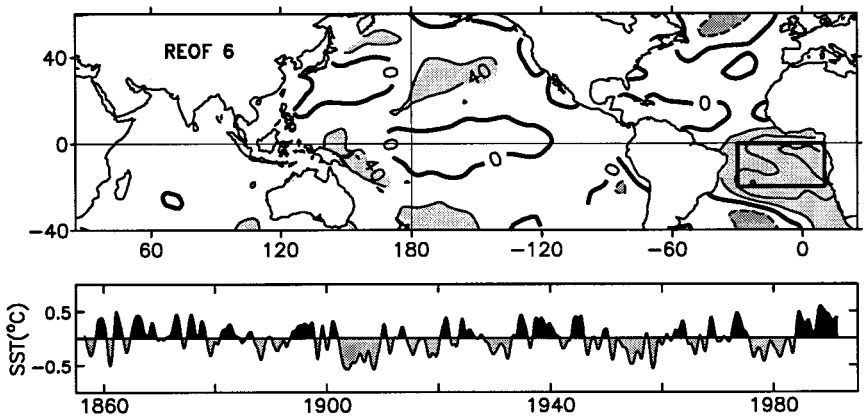

FIG. 6. As in Fig. 1: Sixth REOF of the non-ENSO dataset, describing the South Atlantic interannual variability.

negative response in the South Atlantic in U3. As frequently occurs in unrotated EOF analyses of Atlantic SSTA, the moderate anticorrelation across the equator in U3 gives the impression that an intrinsic physical mode of dipole variability is a significant feature of the basin. However, we found no single rotated mode that shows an Atlantic dipole structure similar to U3. Recall that R1 had large response in the North Atlantic and small response in the South Atlantic. In contrast, R6 has a large response in the tropical South Atlantic but small response in the tropical North Atlantic. Furthermore, the temporal correlation between R1 (North Atlantic) and R6 (South Atlantic) is nearly zero (Table 5), while the local variance explained in each tropical region is significantly greater than in U3. This questions further the existence of any intrinsic Atlantic dipole variability over a wide frequency range.

Enfield et al. (1999) indeed demonstrate that Atlantic dipole configurations occur infrequently and only with chance expectation. They have looked at the R1 and R6 modes presented here in greater detail for the tropical Atlantic. The fact that the two modes are uncorrelated indicates that the large amounts of SSTA variance in the tropical North and South Atlantic are statistically unrelated to each other. However, nondipole configurations associated with meridional SSTA gradients are common. The dipole structure associated with the Sahel rainfall in Folland et al. (1986) is an example of the bivariate relationships of SSTA with anomalies of atmospheric variables that are sensitive to ITCZ latitude and meridional SSTA gradient. Such analyses indicate that gradient–climate covariability is real. They do not mean that dipole configurations of SSTA are a dominant mode of variability, intrinsic or otherwise.

Mode R6 corresponds to the second rotated mode of F91W93, which has been used in empirical seasonal forecasts for Sahel rainfall during the last decade. In the South Atlantic, R6 and mode 2 of F91W93 have very similar structure, including a region of positive response in the western South Atlantic that is beyond the 40°S boundary of our Fig. 6. Mode R6 is also similar to rotated mode 4 of Kawamura, although Kawamura's mode does not show negative loadings in the western South Atlantic at about 30°S. Mode R6 also corresponds to the first mode of Venegas et al. (1997) from an EOF analysis of South Atlantic SSTA for the 40-yr period 1953–92. Similar South Atlantic modes of variability were also found by Houghton and Tourre (1992) and Enfield and Mayer (1997) in their analyses of tropical Atlantic SSTA.

4. Associated atmospheric patterns

The distribution of SLP and surface wind stress associated with the six rotated non-ENSO modes described in section 3 are shown in four three-panel plots (Figs. 7–10). Each SLP or wind stress map is computed by first averaging separately the maps for all months where the corresponding modal time series (bottom panels of Figs. 1–6) were positive or negative, respectively. The final map of each mode is the difference of the positive minus the negative composite for that mode. SLP and zonal wind stress differences that are significantly different from zero at the 95% level are shaded. Significant positive (negative) differences of SLP in Figs. 7–8 and of zonal surface wind stress in Figs. 9–10 are heavily (lightly) shaded.

The SLP pattern associated with R1 (Fig. 7, upper panel) shows significant negative anomalies exceeding 0.8 hPa in the central North Atlantic and larger significant positive anomalies at high northern latitudes. The anomalous cyclonic circulation over most of the North Atlantic is also described by significant surface wind stress anomalies (Fig. 9, upper panel). The anomalous winds show a decrease in the intensity of the northeast trades and a decrease in the intensity of the westerlies over the high latitudes of the North Atlantic. These are both regions of warming in R1. The decrease in the winds is consistent with a decrease in latent and sensible heat fluxes at the surface, suggesting that the temper-

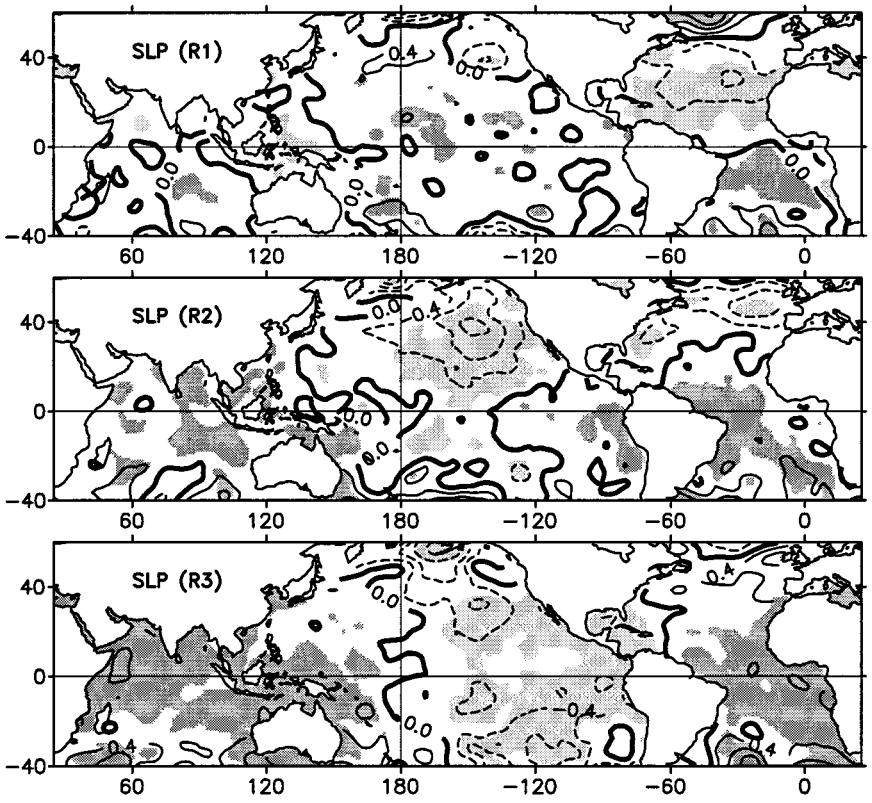

FIG. 7. Difference between composite averages of sea level pressure with respect to positive and negative values of the modal time series in Fig. 1 (upper panel), in Fig. 2 (middle panel), and in Fig. 3 (bottom panel). Contour interval is 0.4 hPa. Significant positive differences are heavily shaded and significant negative differences are lightly shaded.

ature pattern is mostly a response to local forcing by the atmosphere.

The association between the intensity of the westerlies and SSTA suggests a link to the NAO, which has important implications in the weather over Europe (e.g., Hurrel 1995). The SLP pattern, with antinodes in the regions of the Azores high and the Icelandic low, are consistent with the way in which the NAO index is typically computed (Hurrell 1995). The situations shown in Figs. 1 and 7 are diagnostic of the negative phase of the NAO. The relation is such that when there is warming (cooling) over the North Atlantic, the westerlies are weaker (stronger) and the NAO is in its negative (positive) phase. Other features of Fig. 7 (upper) are a low pressure forcing over the Gulf of Alaska and a decrease in the intensity of the Pacific easterlies over smaller regions in the eastern tropical Pacific. The weaker Pacific easterlies seem to correspond to regions of moderate warming.

The SLP and wind stress patterns associated with R2 (Figs. 7 and 9, middle panels) show significant negative pressure anomalies and cyclonic circulation south of the Gulf of Alaska. The northeast trades are weaker over the western and central tropical North Pacific and northward wind anomalies are seen along the west coast of North America. This is consistent with warming due to local surface fluxes in the western and central tropical North Pacific and due to downwelling along the west coast of North America. The pattern (Figs. 7 and 9, middle panels) is consistent, in terms of surface heat, with the northeast Pacific warming pattern seen in R2. If one assumes that the large-scale cyclonic forcing in the eastern Pacific is reflected in a weaker subtropical gyre circulation, it is also consistent with anomalous advection of SST.

Unlike the first two modes, the pattern of SLP and winds for R3 (Fig. 7 and 9, bottom panel) do not suggest an oceanic response to atmospheric forcing in the tropical Pacific. Significant negative pressure anomalies are seen over the region of strong warming in the eastern tropical Pacific and significant positive anomalies over the western tropical Pacific. The anomalous zonal pressure gradient at the equator generates significant eastward wind anomalies near the date line. The pattern is more consistent with an atmospheric response to SSTA due to changes in the Walker circulation. The surface winds also show a southward component over the central and eastern tropical Pacific. The sense of the SSTA–SLP–wind relationship in R3 suggests an oceanic forcing of the atmosphere or perhaps a two-way interaction

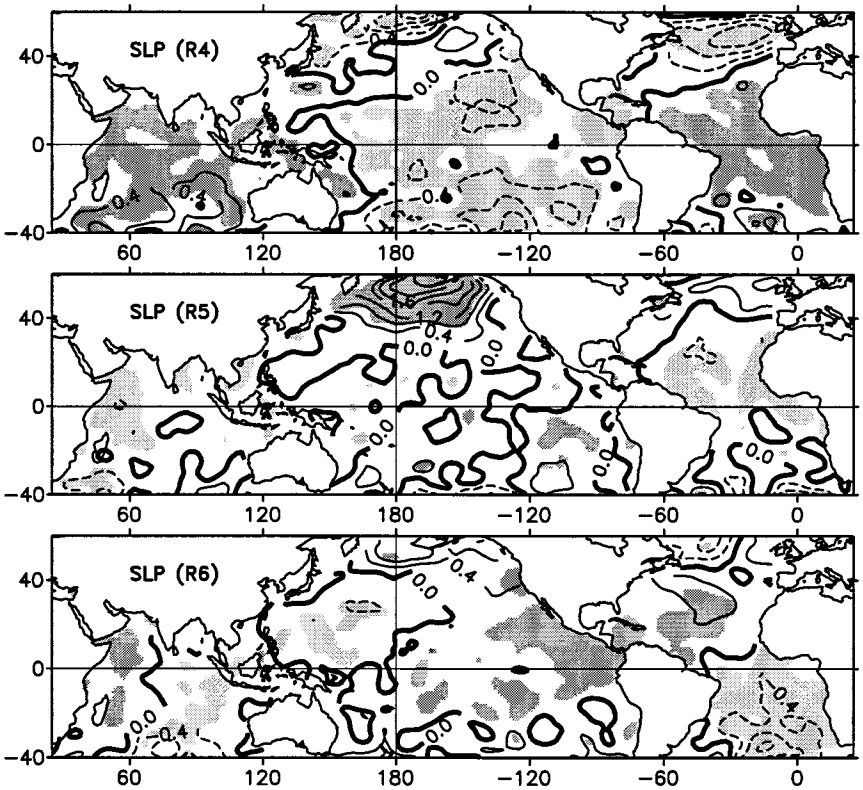

FIG. 8. Same as in Fig. 7 but for the time series in Figs. 4 (upper panel), 5 (middle panel), and 6 (bottom panel).

or feedback, similar to what occurs with ENSO on shorter timescales.

The surface atmospheric patterns associated with R4 (Figs. 8 and 10, upper panels) and R5 (Figs. 8 and 10, middle panels) are discussed together as the two modes seem to be part of the same phenomenon, the PDO. Warming in the central and southestern tropical Pacific (R4) corresponds to a decrease of SLP and a weakening of the trades in those regions. Warming in the northern North Pacific (R5) is associated with anticyclonic forcing over the subpolar low and significant weakening of the midlatitude westerlies.

The pattern of SLP associated with R6 (Fig. 8, bottom) shows significant negative pressure anomalies over most of the South Atlantic. This cyclonic pressure pattern would be consistent with a decrease in the intensity of both the southeast trades and the Southern Hemisphere westerlies. However, the surface winds in the bottom panel of Fig. 10 do not show significant zonal wind anomalies in the South Atlantic, particularly in the northeast where the response of the mode is larger. Venegas et al. (1997) proposed an ocean to atmosphere forcing for their leading South Atlantic SSTA mode. Although our SLP analysis is consistent with local atmospheric forcing in the South Atlantic, our wind analysis does not support this conclusion. The data density for COADS in the South Atlantic is very poor, and Enfield and Mayer (1997) cited this in not finding such relationships. It is interesting to note that while the wind anomalies are not significant in the South Atlantic, they show a significant increase in the intensity of the northeast trades and westerlies in the North Atlantic consistent with the positive phase of the NAO. The way in which an NAO signal would be transmitted to the South Atlantic is an open question. Note also, that although the northeast trades appear intensified, there is no suggestion of cooling in the R6 pattern west of northwest Africa.

5. Summary and discussion

We have performed a varimax rotation of the global non-ENSO SSTA modes of Enfield and Mestas-Nuñez (1999) in an attempt to identify localized centers of variability. The six leading rotated EOF (REOF) modes of variability were used to define regional indexes. For each REOF a region of high spatial amplitude was identified and used to average the SSTA reconstructed from that mode. Away from these index regions, the response of the rotated modes are generally small. The structures of the unrotated modes can be explained as linear combinations of subsets of the regional rotated modes.

The first REOF captures multidecadal fluctuations in the North Atlantic consistent with local atmospheric

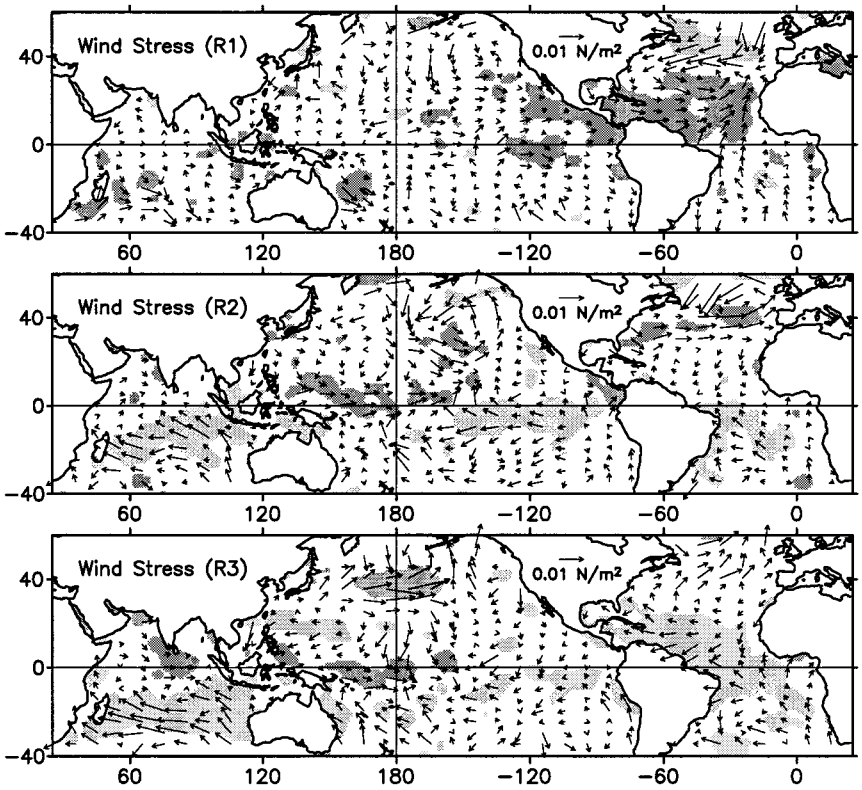

FIG. 9. Difference between composite averages of surface vector wind stress with respect to positive and negative values of the modal time series in Figs. 1 (upper panel), 2 (middle panel), and 3 (bottom panel). Significant positive differences in zonal wind stress are heavily shaded and significant negative differences are lightly shaded.

forcing related to the NAO. The second REOF captures interdecadal fluctuations in the eastern North Pacific related to local atmospheric forcing through surface fluxes and upwelling along the coast of North America. The third REOF captures interdecadal STTA changes in the eastern tropical Pacific that modulate the interannual ENSO. These SSTA changes induce changes in the equatorial Walker circulation that force westward winds in the central equatorial Pacific. The fourth and fifth REOFs capture different aspects of the Pacific interdecadal to multidecadal variability related to the PDO and that are consistent with local atmospheric forcing. The sixth mode is related to interannual changes in the South Atlantic and the comparison with surface pressure suggests a response to atmospheric forcing. However, the wind results are not consistent with this conclusion, which may be due to the poor data coverage of COADS in that region.

In the Atlantic, some discussion of the dipole mode of variability that was captured by the unrotated Atlantic multidecadal mode is required. Our analysis shows that this mode does not hold its structure under rotation—the variabilities north (R1) and south (R6) of the Atlantic ITCZ are described by two different REOFs. These two rotated modes have uncorrelated time series with very different temporal structure. The North Atlantic is dominated by multidecadal scales and the South Atlantic by decadal to interannual scales. Therefore, the results of this study question the existence of a dipole mode of SSTA variability in the Atlantic over a broad range of frequencies, in agreement with Houghton and Tourre (1992), Enfield and Mayer (1997), and Enfield et al. (1999). Note that Kawamura (1994) also found similar North and South Atlantic modes but in that study the modes were constrained to be temporally uncorrelated by the EOF normalization.

In the Pacific, this study supports a description of the non-ENSO SSTA variability as formed of three parts: An eastern North Pacific decadal mode, a PDO-like mode composed of our North Pacific and central tropical Pacific modes, and an eastern tropical Pacific decadal mode. The eastern tropical Pacific decadal mode can be interpreted as a low-frequency modulation to ENSO, as found in other studies (e.g., Zhang et al. 1997). However, our eastern tropical Pacific mode also has interannual variability that may be related to deviations of ENSO from our canonical representation. Known Pacific climatic changes, such as the one that happened in the late 1970s, are evident in our various indexes. These changes appear to be part of the quasiperiodic (decadal and multidecadal) nature of the SSTA variability.

Another important conclusion of this study pertains

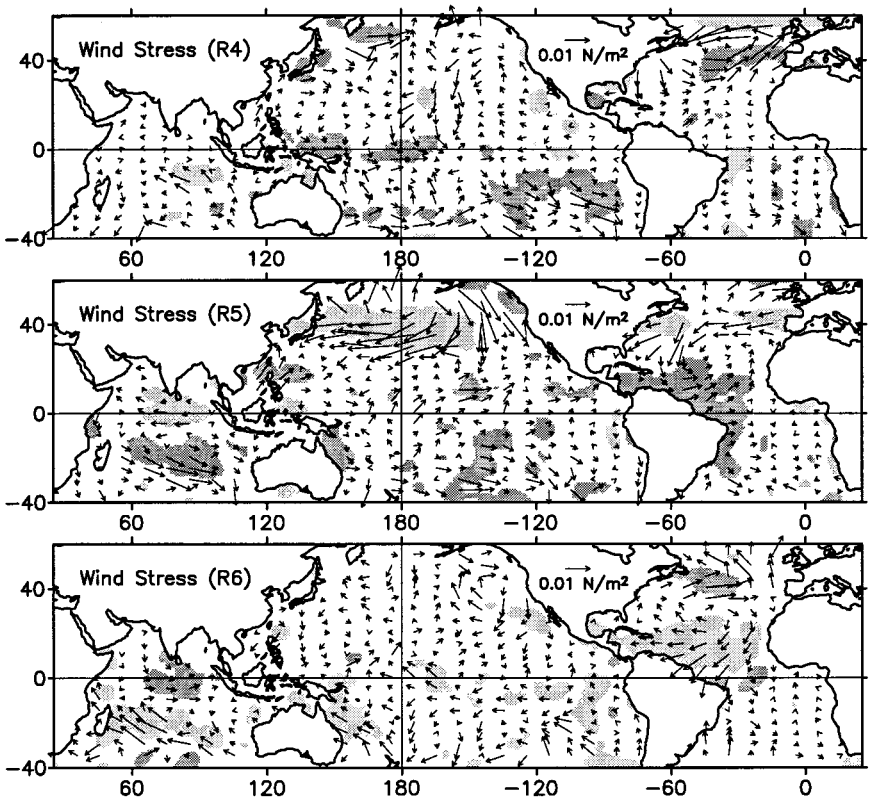

FIG. 10. Same as in Fig. 9 but for the time series in Figs. 4 (upper panel), 5 (middle panel), and 6 (bottom panel).

to the apparent linkage between the North Atlantic and eastern North Pacific non-ENSO SSTA variability. It was shown here that this connection, which was present in the unrotated analysis (U3), is preserved under rotation. The implication is that an atmospheric teleconnection between the North Atlantic and the North Pacific (e.g., through the AO/NAO) may be a real phenomenon.

Acknowledgments. We wish to thank A. Kaplan for making the reconstructed SST dataset available to us and J. Harris for help with the UWM/COADS data. We also thank C. Folland and an anonymous reviewer for helpful comments on an earlier version of this manuscript. Our research has been supported by the National Oceanic and Atmospheric Administration (NOAA) through its Pan-American Climate Studies program, by the Inter-American Institute for Global Change Research (IAI), and by the NOAA Environmental Research Laboratories through their base funding of our laboratory.

REFERENCES

Bottomley, M., C. K. Folland, J. Hsiung, R. E. Newell, and D. E. Parker, 1990: *Global Ocean Surface Temperature Atlas (GOSTA).* Her Majesty's Stationery Office, 20 pp. and 313 plates.

Cardone, V. J., J. G. Greenwood, and M. A. Cane, 1990: On trends in historical marine wind data. *J. Climate,* **3,** 113–127.

da Silva, A. M., C. C. Young, and S. Levitus, 1994: *Atlas of Surface Marine Data 1994.* Vol. 1, *Algorithms and Procedures.* NOAA Atlas NESDIS 6, U.S. Department of Commerce, NOAA, NESDIS, 83 pp.

Deser, C., and M. L. Blackmon, 1995: On the relationship between tropical and North Pacific sea surface temperature variations. *J. Climate,* **8,** 1677–1680.

——, M. A. Alexander, and M. S. Timlin, 1996: Upper ocean thermal variations in the North Pacific during 1970–1991. *J. Climate,* **9,** 1840–1854.

Enfield, D. B., and D. A. Mayer, 1997: Tropical Atlantic sea surface temperature variability and its relation to El Niño-Southern Oscillation. *J. Geophys. Res.,* **102,** 929–945.

——, and A. M. Mestas-Nuñez, 1999: Multiscale variabilities in global sea surface temperatures and their relationships with tropospheric climate patterns. *J. Climate,* **12,** 2719–2733.

——, ——, and D. A. Mayer, 1999: How ubiquitous is the dipole relationship in tropical Atlantic sea surface temperatures? *J. Geophys. Res.,* **104,** 7841–7848.

Folland, C. K., D. E. Parker, and T. N. Palmer, 1986: Sahel rainfall and worldwide sea temperatures 1901–85. *Nature,* **320,** 602–607.

——, J. Owen, M. N. Ward, and A. Colman, 1991: Prediction of seasonal rainfall in the Sahel region using empirical and dynamical methods. *J. Forecasting,* **10,** 21–56.

Giese, B. S., and J. A. Carton, 1999: Interannual and decadal variability in the tropical and midlatitude Pacific Ocean. *J. Climate,* in press.

Gu, D., and S. G. H. Philander, 1997: Interdecadal climate fluctuations that depend on exchanges between the tropics and extratropics. *Science,* **275,** 721–892.

Houghton, R. W., and Y. M. Tourre, 1992: Characteristics of low-

frequency sea surface temperature fluctuations in the tropical Atlantic. *J. Climate,* **5,** 765–771.
Hsiung, J., and R. E. Newell, 1983: The principal nonseasonal modes of variation of global sea surface temperature. *J. Phys. Oceanogr.,* **13,** 1957–1967.
Hurrell, J. W., 1995: Decadal trends in the North Atlantic Oscillation: Regional temperatures and precipitation. *Science,* **269,** 676–679.
Jolliffe, I. T., 1995: Rotation of principal components: Choice of normalization constraints. *J. Appl. Statist.,* **22,** 29–35.
Kaplan, A., M. A. Cane, Y. Kushnir, A. C. Clement, M. B. Blumenthal, and B. Rajagopalan, 1998: Analysis of global sea surface temperatures 1856–1991. *J. Geophys. Res.,* **103,** 18 567–18 589.
Kawamura, R., 1994: A rotated analysis of global sea surface temperature variability with interannual and interdecadal scales. *J. Phys. Oceanogr.,* **24,** 707–715.
Latif, M., and T. P. Barnett, 1996: Decadal climate variability over the North Pacific and North America: Dynamics and predictability. *J. Climate,* **9,** 2407–2423.
Mantua, N. J., S. R. Hare, Y. Zhang, J. M. Wallace, and R. C. Francis, 1997: A Pacific interdecadal climate oscillation with impacts on salmon production. *Bull. Amer. Meteor. Soc.,* **78,** 1069–1079.
Miller, A. J., D. R. Cayan, T. P. Barnett, N. E. Graham, and J. M. Oberhuber, 1994: Interdecadal variability of the Pacific Ocean: Model response to observed heat flux and wind stress anomalies. *Climate Dyn.,* **9,** 287–302.
Nakamura, H., G. Lin, and T. Yamagata, 1997: Decadal climate variability in the North Pacific during the recent decades. *Bull. Amer. Meteor. Soc.,* **78,** 2215–2225.
Nitta, T., and S. Yamada, 1989: Recent warming of tropical sea surface temperature and its relationship to the Northern Hemisphere circulation. *J. Meteor. Soc. Japan,* **67,** 375–383.
Parker, D. E., P. D. Jones, C. K. Folland, and A. Bevan, 1994: Interdecadal changes of surface temperature since the late nineteenth century. *J. Geophys. Res.,* **99,** 14 373–14 399.
Trenberth, K. E., and J. W. Hurrel, 1994: Decadal atmosphere-ocean variations in the Pacific. *Climate Dyn.,* **9,** 303–319.
Venegas, S. A., L. A. Mysak, and D. N. Straub, 1997: Atmosphere–ocean coupled variability in the South Atlantic. *J. Climate,* **10,** 2904–2920.
Ward, M. N., C. K. Folland, K. Maskell, A. W. Colman, D. P. Rowell, and K. B. Lane, 1993: Experimental seasonal forecasting of tropical rainfall at the UK Meteorological Office. *Prediction of Interannual Climate Variations,* J. Shukla, Ed., NATO ASI Series, Vol. 16, Springer-Verlag, 197–216.
Woodruff, S. D., R. J. Slutz, R. L. Jenne, and P. M. Steurer, 1987: A comprehensive ocean atmosphere data set. *Bull. Amer. Meteor. Soc.,* **68,** 521–527.
Zhang, Y., J. M. Wallace, and D. S. Battisti, 1997: ENSO-like interdecadal variability: 1900–93. *J. Climate,* **10,** 1004–1020.